8A.6 QUANTIFICATION OF ERRORS IN POLARIMETRIC RADAR VARIABLES SIMULATED FROM BULK MICROPHYSICS PARAMETERIZATIONS

Matthew R. Kumjian*[1,2,3], Alexander V. Ryzhkov[1,2,3], Scott Ganson[1,4], and Alexander Khain[5]
1. Cooperative Institute for Mesoscale Meteorological Studies, University of Oklahoma, Norman, OK
2. National Severe Storms Laboratory, Norman, OK
3. Atmospheric Radar Research Center, University of Oklahoma, Norman, OK
4. Radar Operations Center, Norman, OK
5. Hebrew University of Jerusalem, Jerusalem, Israel

1. INTRODUCTION

The polarimetric upgrade of the National Weather Service WSR-88D radar network is ongoing. With it comes the ability to remotely interrogate the bulk microphysical properties in a wide array of precipitating systems throughout the diverse climate regions of the United States. This valuable new information can be used to test and validate microphysics parameterizations used in numerical weather prediction models. Such comparisons are possible using polarimetric radar operators (e.g., Pfeifer et al. 2008; Jung et al. 2008a; Ryzhkov et al. 2011), which convert output from the microphysics models into the polarimetric radar variables.

Currently, there are two approaches used to account for cloud and precipitation physics in storm-resolving numerical weather models: bulk parameterizations, where a functional form of the particle size distribution (PSD) is assumed *a priori*, and "bin" or spectral methods, where the number of particles in each size bin is allowed to vary independently via different kinematic and microphysical processes (e.g., see the review by Khain et al. 2000). In bulk schemes, the PSD is often assumed to be in the form of a gamma distribution (e.g., Ulbrich 1983):

$$N(D) = N_0 D^{\alpha} \exp(-\Lambda D) \quad , \qquad (1)$$

where $N(D)$ is the number concentration of particles of diameter D, and N_0, α, and Λ are the intercept, shape, and slope parameters of the distribution, respectively. In many bulk schemes, the shape parameter $\alpha = 0$, resulting in the special case of the inverse exponential distribution. This functional form of the PSD is based on early observations of raindrop size distributions (DSDs) by Marshall and Palmer (1948), and later for snow aggregates by Gunn and Marshall (1958) and hail by Federer and Waldvogel (1975). Changes in the PSD are determined by changes in one or more prognostic moments of the distribution,

*Corresponding Author: Matthew R. Kumjian, 120 David L. Boren Blvd., National Weather Center Suite 4900, Norman, Oklahoma, 73072. E-mail: matthew.kumjian@noaa.gov

$$M_k = \int_0^{\infty} D^k N(D) dD \qquad (2)$$

where M_k is the k^{th} moment. A bulk scheme is characterized by the number of prognostic moments computed; most schemes are single- or double-moment, but more recently a triple-moment scheme has been developed and implemented (e.g., Milbrandt and Yau 2005a,b; 2006a,b). Any combination of moments M_k can be used with varying degrees of accuracy (e.g., Milbrandt and McTaggart-Cowan 2010), though traditionally the moments M_0, M_3, and M_6 have been used. The choice of these moments stems from their relation to common model variables: M_0 is the total number concentration of particles in the category x (N_{TOTx}), M_3 is proportional to the mass mixing ratio of particles (q_x), and M_6 is the Rayleigh reflectivity factor Z_x (assuming spherical liquid water drops). We will consider these prognostic moments for the remainder of the paper.

The next section reviews bulk microphysics schemes and their deficiencies relevant to polarimetric radar observations and applications. Sections 2-7 quantify these errors using a series of explicit bin microphysics models as benchmarks for comparison. Possible implications for future attempts to assimilate polarimetric radar variables into storm-scale numerical weather prediction models are discussed in section 8, followed by brief concluding remarks.

2. BULK MICROPHYSICS SCHEMES

The first parameterization scheme developed for bulk warm rain microphysics was that of Kessler (1969), which uses the inverse-exponential type DSD. The only prognostic moment is the mass mixing ratio; thus, this type of scheme is known as a "single-moment" parameterization. In this type of scheme, with fixed shape parameter ($\alpha = 0$), there are still two parameters in Eqn. (1) but only one prognostic variable. Thus, the intercept parameter N_0 is fixed at the value given by Marshall and Palmer while the slope parameter Λ is allowed to vary with mass mixing ratio.

Later parameterization schemes incorporated the use of ice particles, also with one predictive moment (e.g., Wisner et al. 1972; Ogura and Takahashi 1973; Cotton et al. 1982; Lin et al. 1983). Most of these

schemes used only a few particle types (e.g., the Lin et al. 1983) scheme uses 3 precipitation particle classes: rain, snow, and hail). Improvements to these schemes included the addition of more hydrometeor classes such as the 5 types included in Walko et al. (1995) and the 8 types in Straka and Mansell (2005). Additional hydrometeor classes move the parameterization scheme closer in the direction of the more rigorous spectral model and generally produce more realistic simulated storms.

However, forcing the intercept parameter to remain constant in single-moment microphysics schemes has negative consequences. Even the original work by Kessler (1969) noted that such a constraint "does some violence to the physics of the evaporation process." Indeed, the rate of change of a raindrop's size owing to evaporation is inversely proportional to the raindrop size itself (e.g., Rogers and Yau 1989), so smaller drops evaporate faster than the larger drops and thus are depleted preferentially. This causes the median drop size to increase as evaporation decreases the total mass mixing ratio of rain (converting it into water vapor). Owing to the fixed intercept parameter N_0 in 1M schemes, the evaporation-induced decrease in mass is at the expense of the larger drops, thereby decreasing the median drop size. From a radar perspective, true evaporation causes an increase in Z_{DR} and decrease in Z_H and K_{DP} (Kumjian and Ryzhkov 2010), whereas a 1M bulk scheme produces a decrease in all three variables.

Evaporation is not the only victim of violence when it comes to single-moment (1M) schemes. *Any process that preferentially alters only a portion of the particle size spectrum (especially the smaller sizes) is modeled incorrectly in such a scheme*. Examples of such microphysical processes include melting of hail, freezing of raindrops, and size sorting. Melting can lead to a truncation of the small-size end of the distribution, as smaller particles are preferentially melted more rapidly into rain (e.g., Rasmussen and Heymsfield 1987) leaving only the larger particles. Similarly, the temperature of nucleation and subsequent rate of freezing of raindrops is dependent on drop volume (e.g., Bigg 1953). This leads to an unequal rate of freezing into ice pellets across the size spectrum. Because of the large difference in complex dielectric constant between liquid water and ice, radar observations are strongly affected by the rates of such phase transitions. Size sorting occurs because larger raindrops fall faster than smaller drops (i.e., differential sedimentation), and can lead to a small concentration of large drops and a deficit of smaller drops at low levels beneath a precipitating cloud (Fig. 1a). However, if the intercept parameter is fixed (as in the 1M scheme), the decrease in mass at lower levels is once again incorrectly at the expense of the larger drops (Fig. 1b). As will be shown in the next section, such incorrect treatment of size sorting will result in large errors in the computed polarimetric radar variables.

A major improvement over 1M schemes is the use of a second prognostic moment, which (in most cases) is the total number concentration N_{TOT}, or M_0 (e.g., Ziegler 1985; Cotton et al. 1986; Murakami 1990; Ferrier 1994; Meyers et al. 1997; Reisner et al. 1998; Thompson et al. 2004[1]; Milbrandt and Yau 2005b). Such a configuration allows the added flexibility of varying both the slope and intercept parameters (Λ and N_0), which considerably reduces the mistreatment of certain microphysical processes committed by 1M schemes. However, a major problem with two-moment (2M) schemes that use a fixed shape parameter α is their treatment of sedimentation. Whereas 1M schemes cannot model the process of size sorting, 2M schemes suffer from excessive size sorting (e.g., Wacker and Seifert 2001; Milbrandt and Yau 2005a; Milbrandt and McTaggart-Cowan 2010). This arises from the fact that the moment-weighted fallspeeds for the prognostic variables:

$$V_N = \int_0^\infty v_t(D)N(D)dD \Big/ \int_0^\infty N(D)dD \qquad (3)$$

$$V_q = \int_0^\infty v_t(D)D^3N(D)dD \Big/ \int_0^\infty N(D)D^3dD \qquad (4)$$

$$V_Z = \int_0^\infty v_t(D)D^6N(D)dD \Big/ \int_0^\infty N(D)D^6dD \qquad (5)$$

differ. In eqns. (3) – (5), $v_t(D)$ is the terminal fall speed of a particle of diameter D. Because $V_q > V_N$, sedimentation occurs more rapidly for q, resulting in a flattening of the slope parameter Λ that is not entirely counteracted by the decrease in intercept parameter N_0. This results in an unphysical *increase* in the concentration of large drops (Fig. 1c).

To date, only one triple-moment (3M) scheme has been developed (Milbrandt and Yau 2005b; herein MY05b) and tested in full three-dimensional numerical weather models (MY06a,b; Dawson et al. 2010). In this case, the third prognostic moment is considered the Rayleigh radar reflectivity factor Z ($Z = M_6$). Recall that observed radar reflectivity factor (Z_H) is only equal to the sixth moment of the distribution in the case of small, spherical water particles in the Rayleigh scattering regime (e.g., Doviak and Zrnić 1993; Smith 1984). Use of the third

[1] Note that Thompson et al. (2004) is something of a hybrid, in which only some hydrometeor classes are prognosed with two moments, whereas the rest are treated with single-moment microphysics.

prognostic variable allows the shape parameter α to vary throughout space and time. Such added flexibility allows for a more accurate representation of processes that act to narrow the PSD, such as evaporation and size sorting. However, narrowing of the PSD by increasing α to unrealistically large values can cause an underestimation of the concentration of large drops (Fig. 1d). Because the polarimetric radar variables are especially sensitive to the large particle tail of PSDs, this excessive narrowing of the PSD can result in errors (especially Z_H and Z_{DR}).

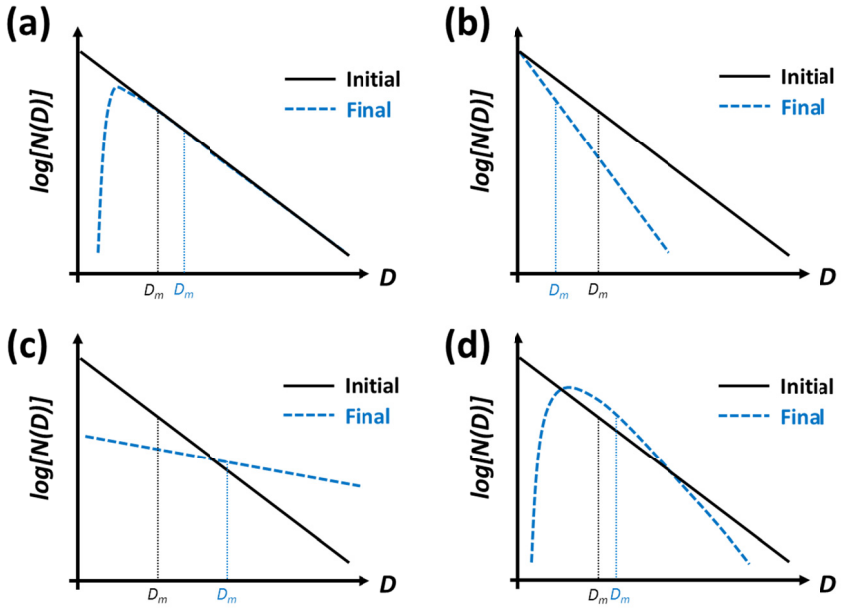

Fig. 1: Schematic cartoon illustrating the sources of error in bulk microphysics schemes handling the process of size sorting. In all panels, the initial PSD is an inverse exponential function (black solid curve), and the resulting PSD after size sorting is shown in the dashed blue line. The initial and final median particle size D_m is annotated on each panel. (a) The true evolution of the PSD, compared to (b) 1M, (c) 2M, and (d) 3M schemes.

3. SEDIMENTATION MODEL

Size sorting of precipitation is a redistribution of particles based on their size (mass). The fundamental process is differential sedimentation, in which the larger (heavier) particles fall faster than smaller particles. Whereas differential sedimentation is a transient phenomenon, size sorting can be maintained by certain atmospheric flows, including updrafts and vertical wind shear (e.g., Kumjian and Ryzhkov 2009; 2012). For the present study, a 1D column model of precipitation fallout is developed. Details can be found in Kumjian and Ryzhkov (2012). The bin formulation divides the initial Marshall-Palmer (1948) DSD into 80 "bins" (0.05 – 7.95 mm in 0.1-mm increments). The fallspeed of each bin size is given by the Brandes et al. (2002) velocity relation, as well as the relation of Uplinger (1981) used in many bulk schemes. In the bulk configuration, moment-weighted fallspeeds (V_N, V_q, V_Z from eqns. 3 – 5) are used in the sedimentation of each moment, which is governed by

$$\frac{\partial N_{TOT}}{\partial t} - V_N \frac{\partial}{\partial z}(N_{TOT}) = 0 \quad (6)$$

$$\frac{\partial q}{\partial t} - \frac{1}{\rho_{air}} V_q \frac{\partial}{\partial z}(\rho_{air} q) = 0 \quad (7)$$

$$\frac{\partial Z}{\partial t} - V_Z \frac{\partial}{\partial z}(Z) = 0 \quad (8)$$

Figure 2 is an example of model output at t = 333 seconds at two height levels. It is clear from the bin model solutions that the DSD has substantially narrowed owing to size sorting. At 1000 m AGL (Fig. 2a), the 1M and 2M schemes poorly match the "true" bin solutions. On the other hand, the 3M scheme better approximates the narrowing effect of size sorting. However, while narrowed, the 3M solution still underpredicts the largest drops and overpredicts smaller drops. Neither the 1M nor 2M solutions have rain reaching the ground at this time (Fig. 2b), whereas the 3M scheme does.

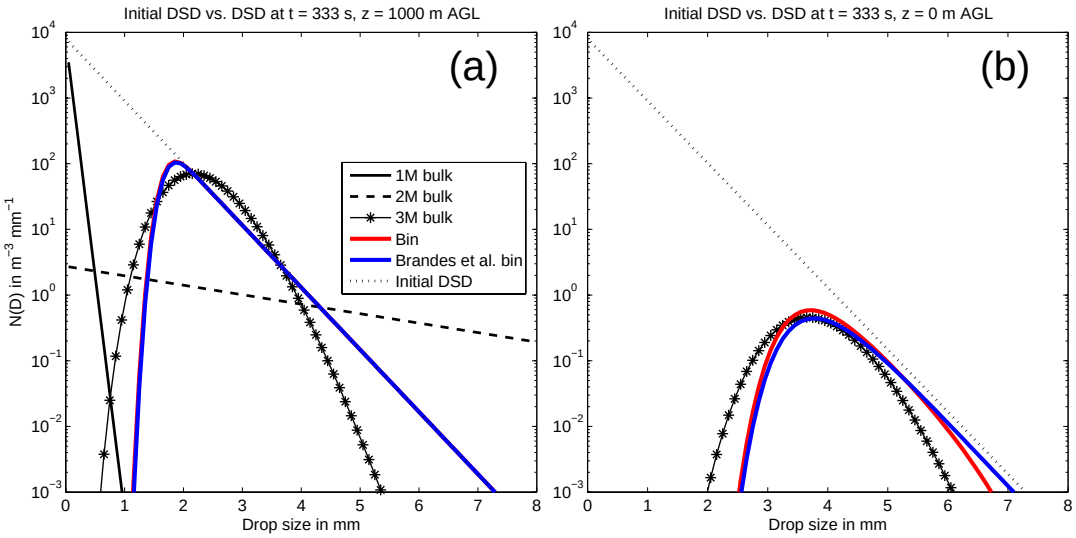

Fig. 2: DSDs from the sedimentation model. The initial DSD aloft is shown by the thin dotted line in both panels. (a) At t = 333 s, at height level z = 1000 m AGL, the 1M bulk scheme solution is given by the solid black line, the 2M solution is given by the dashed black line, and the 3M scheme solution is shown in the solid line with asterisk markers. The reference bin solutions are shown in solid red and blue lines, the difference being the assumed fall speed relation. (b) As in (a), but surface (z = 0 m) DSDs at t = 333 s from the reference bin solutions. Note that in (a), the bin solutions overlap.

How do errors in the DSD shape affect the polarimetric radar variables? Figure 3 displays vertical profiles of all polarimetric radar variables. As expected from the substantial disagreements in the 1M and 2M predicted DSDs, the vertical profiles of the S-band polarimetric radar variables predicted by the 1M and 2M model schemes also differ significantly (Fig. 3). In the Z_H profile (Fig. 3a), neither the 1M or 2M bulk schemes' rain shafts has reached the surface, whereas the surface Z_H from the bin solutions is about 36 dBZ. The 3M scheme provides a rather close agreement to the bin solutions, underestimating the Z_H by about 2 dBZ at the ground. At midlevels, the 2M scheme overpredicts Z_H by nearly 10 dBZ, whereas the 1M and 3M schemes match well (< 1 dBZ error). Predominantly, the 2M error is because of the excessive number of large drops (which strongly affect Z_H) produced. Note that where $Z_H \leq 0$ dBZ, all radar variables have been censored to emulate a minimum detectable radar signal.

The profiles of Z_{DR} (Fig. 3b) are perhaps the most revealing. The 1M solution predicts an accurate profile down to about 1 km AGL, but is entirely wrong below 1 km, owing to a lack of any drops able to fall below that level. Thus, Z_H and Z_{DR} decrease sharply at the leading edge of this "shockwave." The inability to capture the size sorting is due to the use of a single prognostic moment; all variables of interest are a single-valued function of q, and because q does not reach the ground, Z_{DR} (and all of the radar variables) follows the same pattern. In stark contrast, the 2M scheme produces excessive "size sorting," resulting in an overprediction of Z_{DR} by over 2.5 dB (a relative error of 168%) at midlevels and towards the bottom of the rain shaft. The simulated Z_{DR} values reach the upper limit (about 4 dB) because of the truncated DSD used to calculate the polarimetric variables; otherwise, Z_{DR} values could far exceed those observed at S band as unrealistically large (and presumably oblate) drops would be produced. The 3M scheme Z_{DR} profile is closer to the bin solutions, though still underestimates Z_{DR} by almost 0.5 dB (about 25% relative error). The 3M errors will be discussed in more detail below. Though the reference solutions are similar to one another, the Brandes et al. (2002) velocity relation predicts a surface Z_{DR} value 0.15 dB larger than the power-law relation used in bulk schemes. The increase in Z_{DR} at the surface over the initial value aloft is over 1.0 dB for both bin solutions, illustrating the ability of size sorting to substantially enhance Z_{DR} values in rain.

The profiles of K_{DP} (Fig. 3c) produced by the 1M and 2M solutions also show the shock wave problem, albeit smoothed by the diffusive finite differencing scheme used in this model. The 2M bulk scheme produces a midlevel relative maximum in K_{DP}, causing a dramatic overprediction compared to the bin solution (relative error of 217%), whereas the 1M scheme's maximum overprediction of K_{DP} is only about 10%. The 3M scheme overpredicts K_{DP} at midlevels, with a maximum relative error of 24%. The reference solution smoothly varies in height and

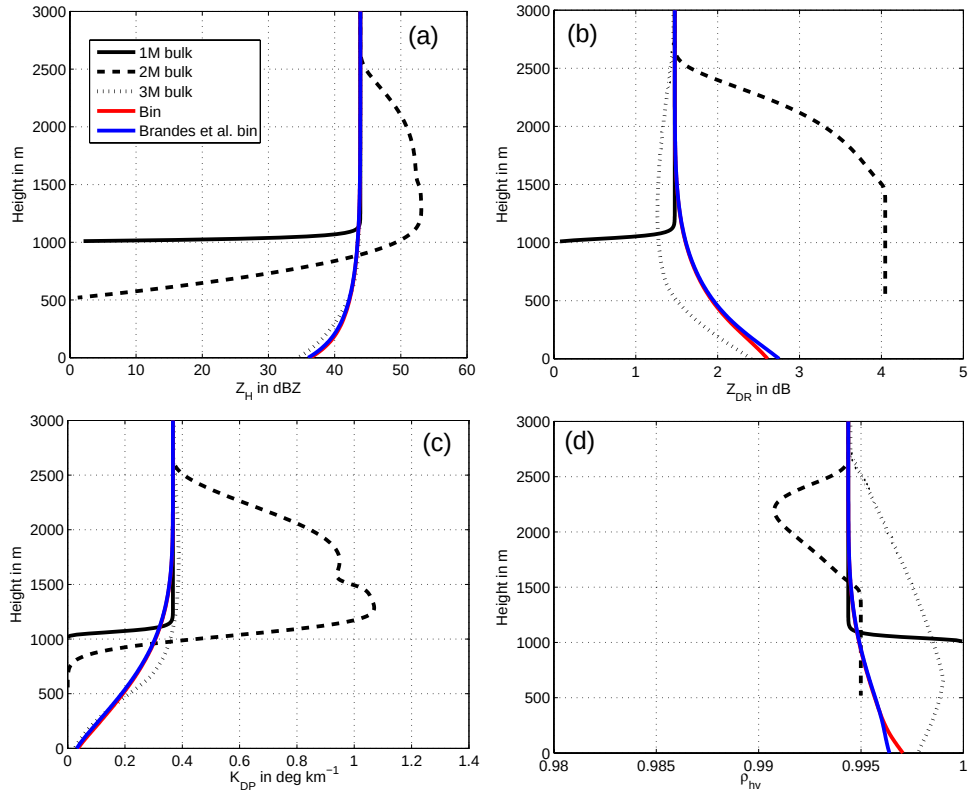

Fig. 3: Vertical profiles of the S-band polarimetric radar variables predicted by the sedimentation model at t = 333 seconds. The solutions for the one-moment (solid black line), two-moment (dashed black line), and three-moment (dotted black line) bulk schemes are compared to the reference solutions (red and blue solid curves). Variables shown are calculated for S band: (a) Z_H, (b) Z_{DR}, (c) K_{DP}, and (d) ρ_{hv}. For the bulk schemes, all variables are censored where $Z_H \leq 0$ dBZ.

both velocity relations produce nearly identical results. Though differences exist in the profiles of ρ_{hv} (Fig. 3d), the changes are small in magnitude at S band (all variations are < 0.01) and likely are not measurable. At smaller radar wavelengths, resonance scattering associated with large raindrops (5-6 mm at C band, 3-4 mm at X band) could exacerbate the errors to the extent that they become measurable.

During sedimentation of the sixth moment Z in the 3M scheme, the shape parameter α can grow to unrealistically large values. Disdrometer observations generally do not reveal α larger than about 15 – 20 (e.g., Zhang et al. 2001; Cao et al. 2008). The microphysics scheme of MY05b limits α to a maximum of α_{max} = 40 (D. Dawson, 2011 personal communication), which is what we have adopted in the present study. Varying this upper limit to α changes the error characteristics, especially at the bottom of the rain shaft (Fig. 4). Whereas the magnitudes of the relative errors in Z_H are < 5%, larger errors (> 20%) are possible in Z_{DR} and K_{DP}. Above 1 km AGL (Figure 4b), Z_{DR} errors become increasingly negative, which indicates under-estimations for all values of α_{max}. This is because narrowing the DSD by increasing α leads to a decrease in the number of small drops (which is physically consistent with size sorting) *as well as* a decrease in the number of large drops (which is inconsistent; c.f. Figure 2a). Thus, Z_{DR} is underestimated. Below 1 km, at the very bottom of the rain shaft, the ability of the 3M scheme to reproduce the "true" Z_{DR} profile depends on α_{max}. Limiting α_{max} to 10 results in an overprediction of Z_{DR} near the ground, because once the α_{max} is achieved, the additional size sorting is represented by decreasing the slope parameter Λ, as in the 2M scheme. The vertical profiles of relative errors in K_{DP} (Figure 4c) demonstrate similar behavior, but of opposite sign. The increasingly positive errors (overestimations) result from an artificial increase in the number medium-sized drops, which can be seen in Figure 2a. Based on the excessive narrowing of the DSD that occurs for large α_{max} demonstrated above, it is recommended to use more rigid constraints (e.g., α_{max} = 20.0 – 30.0) for the 3M scheme, especially for polarimetric radar applications.

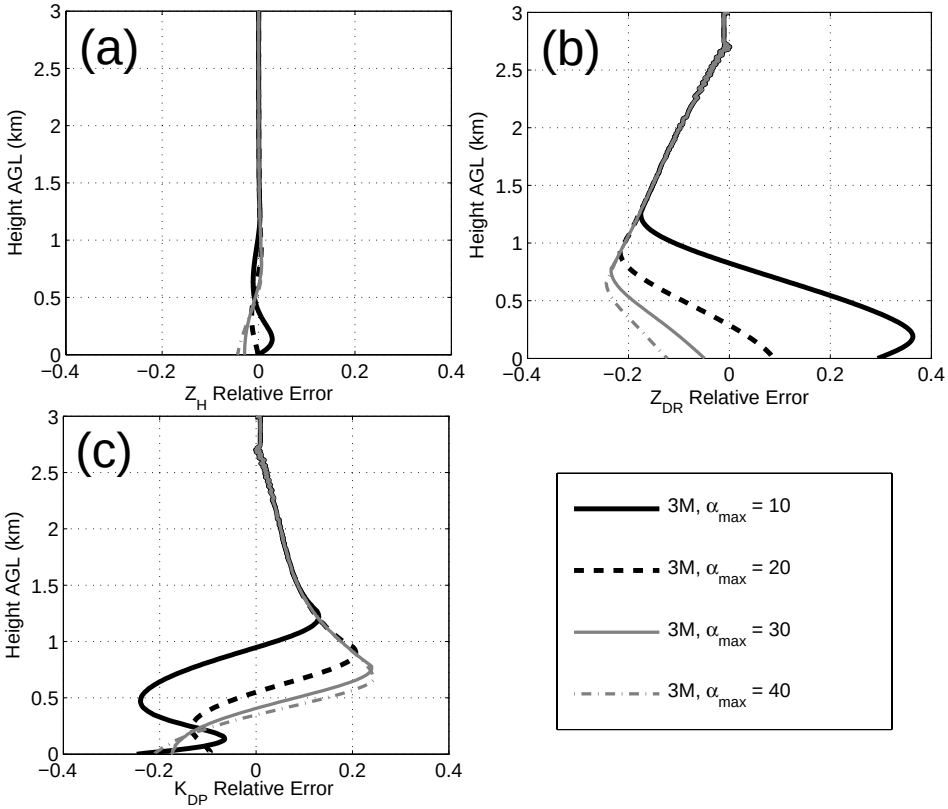

Fig. 4: Relative errors in the polarimetric variables computed from the three-moment scheme with different values of maximum shape parameter α: 10 (black solid line), 20 (dashed black line), 30 (solid gray line), and 40 (dash-dot gray line). Variables shown are (a) Z_H, (b) Z_{DR}, and (c) K_{DP}. The Brandes et al. bin solution is considered "truth" for these error calculations. Positive errors correspond to overestimations by the 3M scheme, negative errors to underestimations.

4. WIND SHEAR MODEL

In addition to pure differential sedimentation, precipitation falling into sheared flow also will undergo size sorting, as the faster-falling particles encounter stronger flow for a shorter duration than the slower-falling particles. This type of size sorting results in an enhancement of Z_{DR} along the leading edge of the precipitation shaft, typically along a gradient in Z_H. The model developed herein follows Kumjian and Ryzhkov (2012), and considers a steady-state shaft encountering constant shear of $6.66 \cdot 10^{-3}$ s^{-1}, where precipitation particles follow trajectories governed only by sedimentation and advection:

$$u(z)\frac{\partial}{\partial x}[N(D)] + v_t(D)\frac{\partial}{\partial z}[N(D)] = 0, \quad (9)$$

where $u(z)$ is the storm-relative flow as a function of height. For the bulk schemes, v_t is replaced by the moment-weighted fallspeeds (eqns. 3-5).

Figure 5 shows output of the wind shear model in the bin configuration. Aloft, the rainfall rate in the cloud is modulated as a Gaussian distribution with maximum Z_H and Z_{DR} in the center. However, after encountering the wind shear, the highest Z_{DR} at low levels is now located at the leading edge, along a gradient of Z_H. Of note is that the Z_{DR} at the leading edge is higher (36%) than anywhere in the cloud aloft; this demonstrates the ability size sorting to amplify the Z_{DR} in precipitating systems. As expected, large errors are present in the simulated Z_{DR} from the 1M and 2M schemes (Fig. 6a,b), whereas errors in the 3M (Fig. 6c) are much smaller (< 0.5 dB). Much of the domain reveals positive differences for the 1M scheme (Fig. 6a), indicating underestimations of Z_{DR} as much as 1.5 dB. The overestimations by the 2M scheme (Fig. 6b, negative differences) are > 2 dB in magnitude.

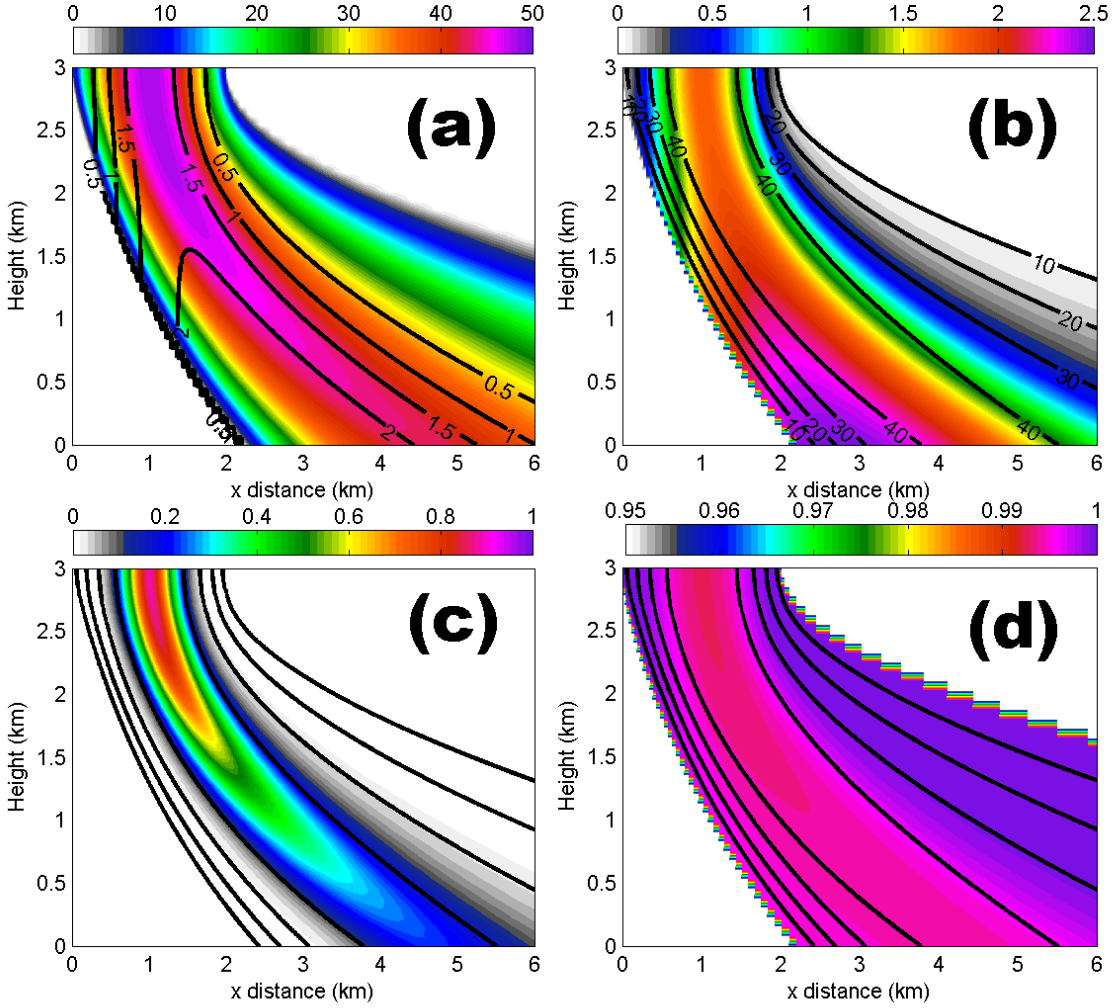

Fig. 5: Results from the two-dimensional wind shear model using the bin formulation. Panels show the two-dimensional fields of (a) Z_H, (b) Z_{DR}, (c) K_{DP}, and (d) ρ_{hv}. Overlaid on panel (a) is the Z_{DR} contours (0.5 – 2.5 dB in 0.5 dB increments), whereas panels (b)-(d) have Z_H contours 10 – 40 dBZ (in 10-dBZ increments) overlaid. For Z_H < 0 dBZ, all fields are set to zero.

5. EVAPORATION MODEL

As discussed above, evaporation of raindrops preferentially affects the smallest drops in the distribution. Over time, this can lead to a narrowing of the DSD, resulting in changes in the polarimetric radar variables similar to those incurred by size sorting, though of lesser magnitude (e.g., Kumjian and Ryzhkov 2010). Because of assumptions made to simplify the physics of evaporation in some bulk microphysics schemes (e.g., MY05b), we focus here on the errors incurred *solely from the assumed functional form of the DSD*. Thus, the explicit microphysics model of Kumjian and Ryzhkov (2010) is used for both the bin and bulk solutions.

Output from the bin solution is converted to the moments q and N_{TOT} as follows. For the 1M scheme, q is calculated by summing the 3rd moment of the discretized DSD (with n drop size bins) as

$$q = \frac{\pi \rho_w}{6 \rho_{air}} \sum_{i=1}^{n} N(D_i) D_i^3 \Delta D \quad . \tag{10}$$

The slope parameter Λ is then determined from

$$\Lambda = \left(\frac{\pi \rho_w}{q \rho_{air}} N_0 \right)^{\frac{1}{4}} \quad , \tag{11}$$

where ρ_w and ρ_{air} are the densities of water and air, respectively, and N_0 here is the intercept parameter for

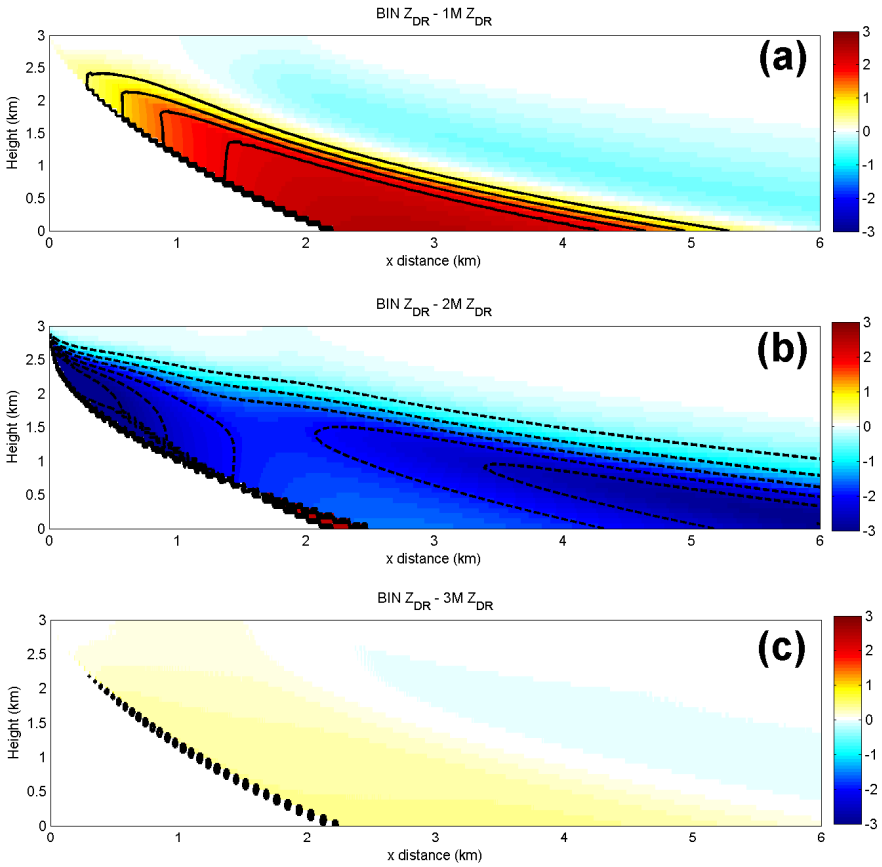

Fig. 6: Z_{DR} difference fields between (a) the bin model and the 1M bulk scheme, (b) the bin model and the 2M bulk scheme, and (c) the bin model and the 3M bulk scheme. Contours in 0.5-dB intervals are overlaid (solid lines for positive differences, dashed lines for negative).

the Marshall-Palmer distribution (= 8000 m^{-3} mm^{-1}). For the 2M scheme, N_{TOT} is calculated from

$$N_{TOT} = \sum_{i=1}^{n} N(D_i)\Delta D \quad . \tag{12}$$

The intercept parameter for the 2M scheme is defined as

$$(N_0)_{2M} = N_{TOT}\Lambda_{2M}, \tag{13}$$

which is substituted into the definition of mass mixing ratio q:

$$q = \frac{\pi}{6}\frac{\rho_w}{\rho_{air}}\frac{\Gamma(4)N_0}{\Lambda_{2M}^4} = \pi\frac{\rho_w}{\rho_{air}}\frac{N_{TOT}}{\Lambda_{2M}^3}. \tag{14}$$

Eqn. (14) is then solved for Λ_{2M}, which is finally used to determine $(N_0)_{2M}$ using eqn. (13).

The calculations are performed for an idealized well-mixed layer, with a surface temperature of 30 °C and surface relative humidity of 60%. Both the relative humidity and temperature change linearly with height to the "cloud base" at 3km to 100% and 0 °C, respectively. The atmospheric pressure is determined using the Norman sounding from Kumjian and Ryzhkov (2010), and density is calculated from the ideal gas law. A Marshall-Palmer DSD with rainfall rate of 5 mm hr^{-1} is initialized aloft.

Figure 7 is a four-panel display of vertical profiles of the polarimetric variables computed from the evaporation model output. As expected, the 1M scheme overestimates the changes in Z_H owing to evaporation, removing large drops rather than small drops. The surface Z_H from the 1M scheme is about 6 dBZ lower than the bin solution. In contrast, the 2M scheme initially increases Z_H aloft before decreasing towards the ground. The resulting surface value of Z_H in the 2M scheme is 5 dBZ too high. Whereas the bin solution Z_{DR} increases slightly towards the ground, the 1M scheme results in a *decrease* in Z_{DR} towards the ground, opposite of the true physics. As with size sorting, the increase in Z_{DR} in the 2M scheme is exaggerated, overpredicting the surface Z_{DR} value by nearly 0.8 dB. The 1M change in K_{DP} is exaggerated and the 2M profile incorrectly increases K_{DP} initially, similar to the errors in the Z_H profiles. Though

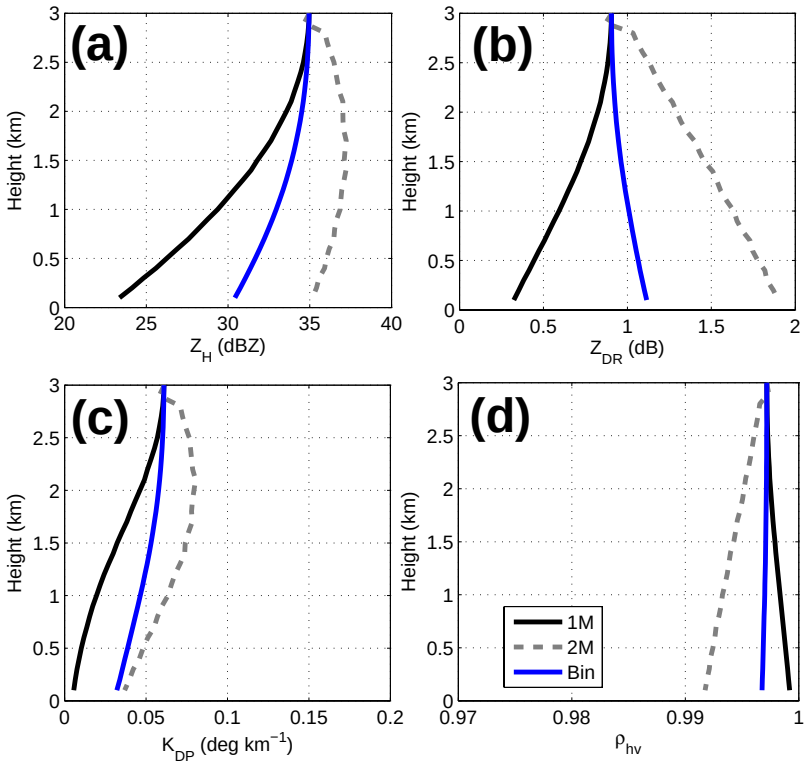

Fig. 7: Vertical profiles of the polarimetric variables computed from the evaporation model. Variables shown are (a) Z_H, (b) Z_{DR}, (c) K_{DP}, and (d) ρ_{hv}. The solid black line depicts the 1M solution, the dashed gray line is the 2M solution, and the bin ("truth") solution is shown in the solid blue line.

changes in ρ_{hv} are of the wrong sign in the 1M scheme and exaggerated in the 2M scheme, the magnitude of changes in all solutions is less than what is detectable by operational WSR-88D radar.

6. FREEZING MODEL

Kumjian et al. (2010a) developed a simplistic one-dimensional explicit bin model describing the freezing of raindrops in convective updrafts, atop the Z_{DR} column. Drops are lofted above the freezing level, whereupon they undergo stochastic nucleation in the immersion mode (e.g., Pruppacher and Klett 1997). Freezing of the nucleated drops then proceeds from the outside inwards until all liquid water is converted to ice. In the electromagnetic model used for the scattering calculations, the partially frozen drops ("slush" particles) are considered two-layer spheroids, with an ice shell and liquid water interior. The model is capable of reproducing several observed features atop Z_{DR} columns in convective storms, including the appropriate rate of decrease of Z_H, the magnitude and slope of the Z_{DR} decrease, and a minimum in ρ_{hv} in the freezing zone (Fig. 8).

Partially-frozen "slush" particles are generally not considered in bulk microphysics parameterizations. A notable exception is the recent work by Thériault and Stewart (2010), who consider numerous classes of mixed phase particles in their winter precipitation parameterization. In most bulk schemes, raindrops freeze by a combination of probabilistic and collisional processes when lofted above the environmental freezing level; mass from the raindrop category is converted directly to the "frozen drops/hail" category, skipping the "slush" stage. Aircraft observations (e.g., Smith et al. 1999; Loney et al. 2002; Clabo et al. 2009) have reported mixed-phase particles in Z_{DR} columns above the freezing level. These mixed-phase particles substantially affect the observed polarimetric variables, as the presence of liquid water in or on a mixed-phase particle increases its Z_{DR} and can contribute to decreased ρ_{hv} and increased LDR (e.g., Jameson et al. 1996; Bringi et al. 1997; Hubbert et al. 1998).

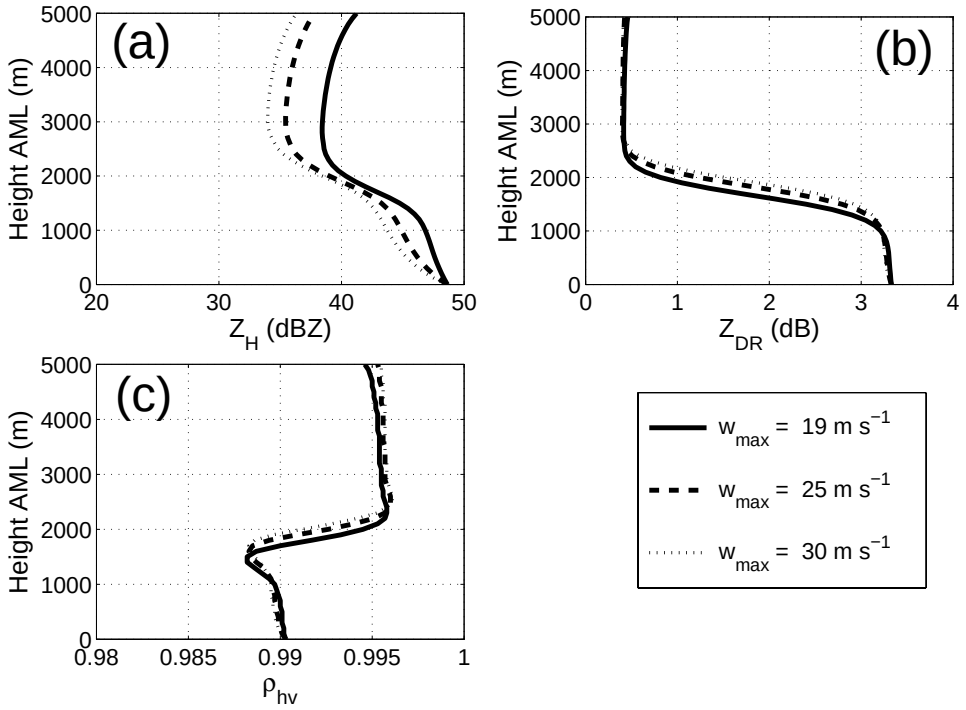

Fig. 8: Vertical profiles of (a) Z_H, (b) Z_{DR}, and (c) ρ_{hv} computed from output of the freezing model of Kumjian et al. (2010a), shown in meters above the melting level (AML). The model parameters used for the calculations include the default DSD with varying updraft maximum intensity: 19 m s^{-1} (solid curves), 25 m s^{-1} (dashed curves), and 30 m s^{-1} (dotted curves). These calculations are for S band, employing the Rayleigh approximation.

For the analysis, simulated PSDs from 1.7 km above the freezing level are selected. At this altitude, particles of the same size but different species coexist with different distributions (Fig. 9). Results of scattering calculations from the bin model along with those from the 1M and 2M bulk configurations with fixed $\alpha = 0$ are presented in Table 1. The intercept parameter for frozen drops from Straka and Mansell (2005; $4 \cdot 10^2$ m^{-3} mm^{-1}) is used. Both bulk schemes dramatically underestimate Z_H, and both underestimate Z_{DR}, largely because of undercounting of the larger particles compared to the bin solutions. Also of note is the "exotic" shape of the bin solution PSDs, especially for raindrops. These unusual PSD shapes are not well captured by inverse exponential distributions. Introducing gamma functions with variable shape parameters may help better approximate the bin solutions.

These results have implications for the ability of bulk microphysics schemes to reproduce observed features of Z_{DR} columns; without the intermediate "slush" category, liquid water may be frozen too rapidly, limiting the height of the top of the Z_{DR} column. Additionally, the lack of diversity of particle types coexisting at a particular grid point will produce erroneously high ρ_{hv} values. Indeed, most bulk schemes fail to reproduce tall Z_{DR} columns or appreciable wet hydrometeors well above the freezing level (e.g., Lin et al. 1983; Ferrier et al. 1995; MY06a,b; Jung et al. 2010). This inability of bulk microphysics schemes to simulate significant Z_{DR} columns (or water above the freezing level), along with the calculations and radar observations strongly suggest the need to include a mixed-phase particle category such as partially-frozen drops or slush, as in Thériault and Stewart (2010). Improving microphysics schemes in this way may allow modeling studies to further explore the short-term predictability of Z_{DR} columns recently revealed by Picca et al. (2010).

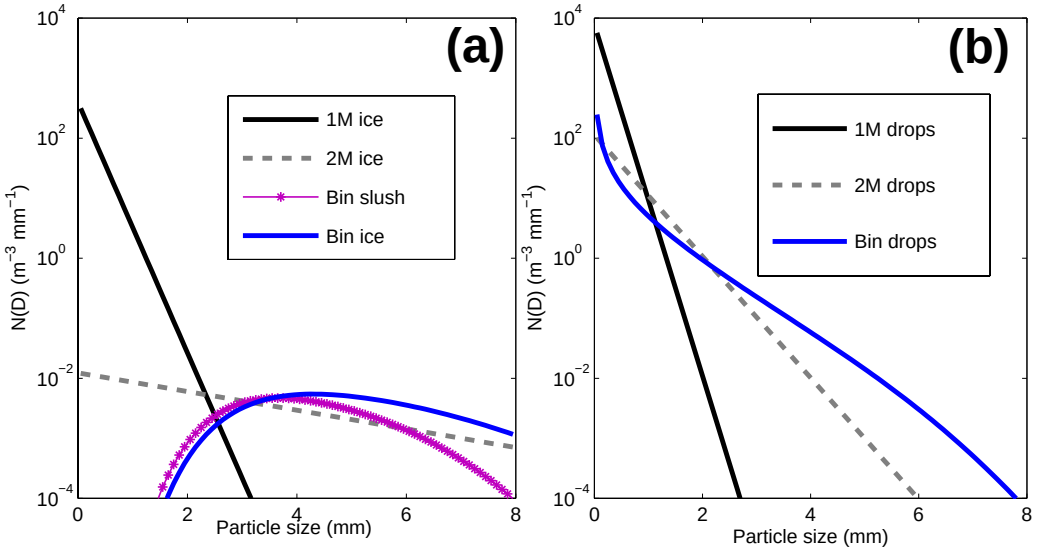

Fig. 9: Simulated particle size distributions from the one-dimensional freezing model of Kumjian et al. (2010a), taken from the height level 1.7 km above the freezing level. (a) Ice species, with the 1M and 2M schemes simulated PSDs of frozen drops (black solid and gray dashed curves, respectively), and the bin "slush" particles (magenta line with markers) and frozen drops (blue solid line). (b) Liquid drops from the 1M (black solid curve), 2M (dashed gray curve), and bin model (blue solid curve).

Model	Z_H total (dBZ)	Z_{DR} total (dB)
Explicit Bin	41.8	2.26
One Moment	9.7	0.14
Two Moment	24.7	1.47

Table 1: Computed values of the polarimetric variables at 1.7 km above the 0 °C level in the Kumjian et al. (2010a) freezing model, from the explicit bin distributions as well as the 1M and 2M approximations. Calculations here employ the Rayleigh approximation.

7. HEBREW UNIVERSITY CLOUD MODEL

The next stage in the analysis employs the two-dimensional explicit spectral microphysics Hebrew University Cloud Model (HUCM; e.g., Khain et al. 2004). This more sophisticated treatment of microphysics provides arguably more realistic PSDs than the idealized models presented above. The simulated storm (Fig. 10) is initialized using the afternoon sounding from 10 February 2009. The observed storms on that day produced giant hail (> 7 cm in diameter) and several tornadoes (see Ryzhkov et al. 2011). Being a two-dimensional model, the HUCM is incapable of producing a tornadic supercell storm; however, the simulated storm is quite strong and produces abundant large hail (e.g., Ryzhkov et al. 2011; Kumjian et al. 2010b). Sixty grid cells at low levels (0.75 km AGL) and fifty at midlevels (4.65 km AGL) are selected for the analysis (black points in Fig. 10). The particle size distributions (PSDs) for rain, hail, and graupel at each grid cell are used to compute the polarimetric variables. The PSDs taken directly from the HUCM are considered "truth" in comparisons with the distributions obtained using assumptions of bulk microphysics schemes. Thus, relative errors in the polarimetric variables are calculated with respect to those obtained using the HUCM distributions.

Figure 11 is a series of Z_H-Z_{DR} plots from rain DSDs in the HUCM storm for various fixed values of α. Immediately evident is the trend in single-moment data points, which demonstrates that Z_{DR} is a single-value function of Z_H owing to the use of a single prognostic variable. Also evident is the shift down and to the left (towards lower Z_{DR} and Z_H values) for the two-moment points as the value of α is increased. The 2M data compare favorably to the "truth" values from the bin model only for the lowest α values. In fact, the standard fixed value α = 2.5 used in many 2M schemes (e.g., Ferrier 94) is noticeably a worse match to the bin model. Therefore, MY05b's constraint of $\alpha \geq 2.0$ everywhere in rain may be too restrictive.

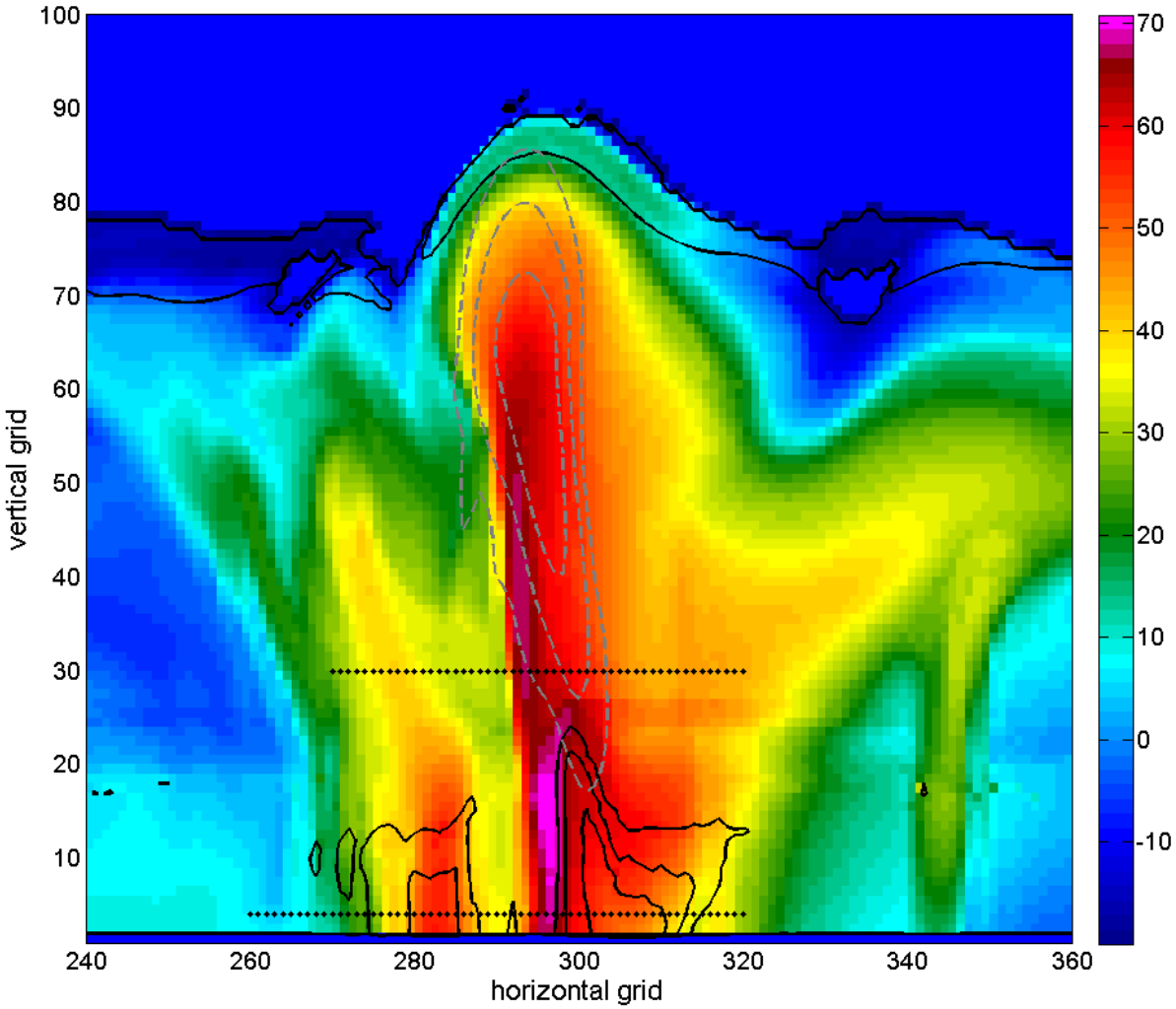

Fig. 10: Simulated radar Z_H (color shading, in dBZ), Z_{DR} (solid black contours), and updraft speed (gray dashed contours). The black points represent grid cells selected for the analysis. Z_{DR} contours start at 2 dB with a 2-dB contour interval; updraft speed contours every 10 m s^{-1}, starting at 10 m s^{-1}. Horizontal grid spacing is 0.35 km, vertical grid spacing is 0.15 km.

The error characteristics of dry hail aloft in the HUCM storm are considered next (Fig. 12). The C- and X-band Z_{DR} and ρ_{hv} values are negatively biased, with the most noticeable errors at X band. For example, many of the bin model hail size distributions produce slightly positive Z_{DR} values, but the bulk schemes produce pronounced negative Z_{DR}. All particles are modeled as oblate spheroids, so the negative Z_{DR} values are an indication of non-Rayleigh scattering. Whereas the bin model ρ_{hv} does not drop below about 0.985 for the dry hail aloft (at X band), the bulk scheme distributions produce X-band ρ_{hv} values as low as 0.95.

The anomalously low values of ρ_{hv} and the negative Z_{DR} in pure dry hail arise in part from overcounting of the larger resonance-sized particles. The particle diameter for which Mie scattering effects are pronounced is ascertained from where the resonance parameter,

$$\mathcal{R} = D\sqrt{|\varepsilon|}/\lambda \qquad (15)$$

approaches unity. In eqn. (15), ε is the complex dielectric function and λ is the radar wavelength. For scatterers comprising solid ice, the resonance size is about 3.0 cm (1.8 cm) for C band (X band). Resonance-sized particles contribute to decreased ρ_{hv} because of their intrinsic nonzero differential phase

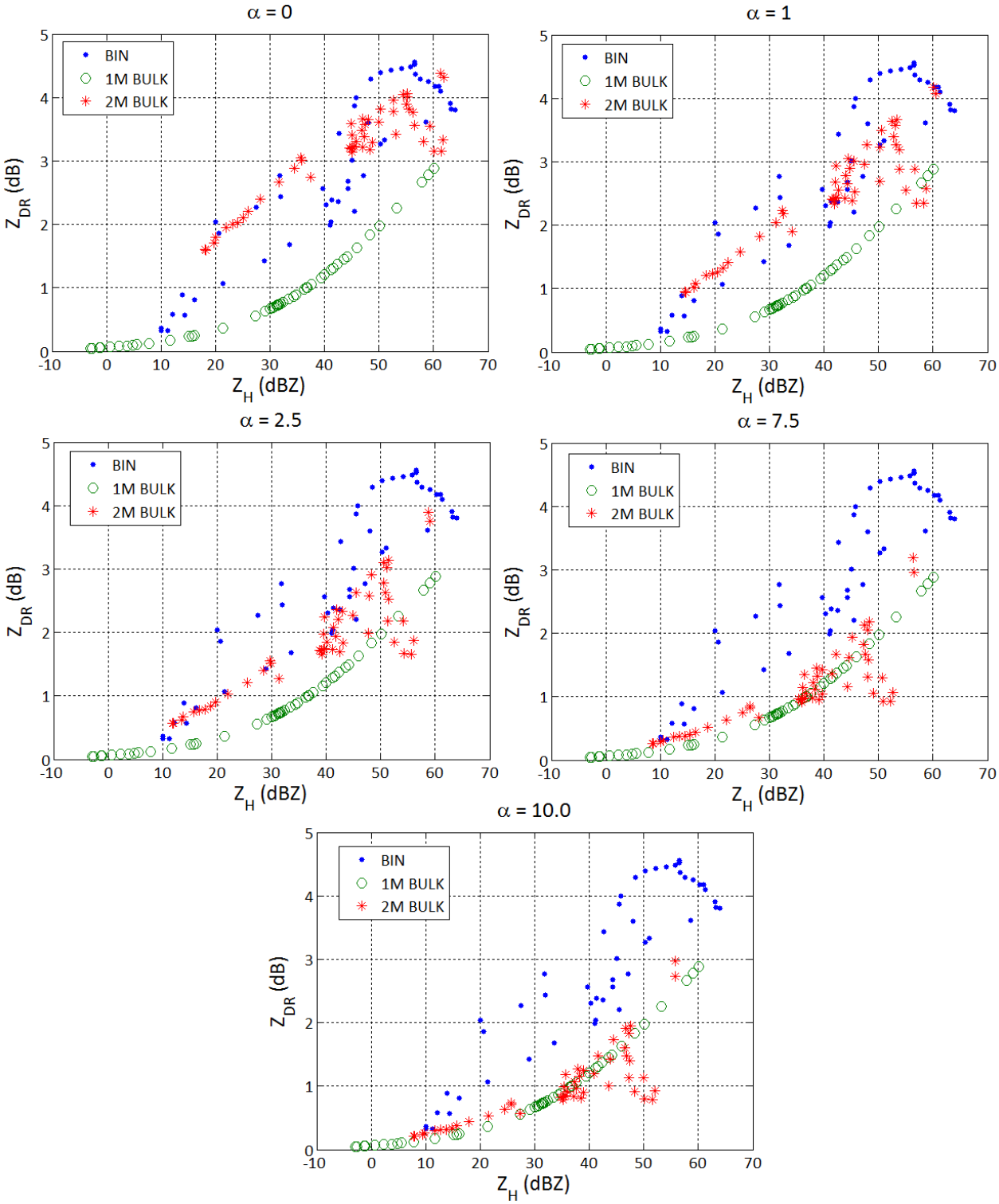

Fig. 11: Z_H-Z_{DR} scatterplots from rain DSDs at low levels in the HUCM storm. The S-band variables are calculated from the HUCM distributions (blue points), the one moment scheme DSD (green circles), and the two-moment scheme DSDs (red asterisks). Calculations are repeated for various values of fixed shape parameter α (from top left, 0, 1.0, 2.5, 7.5, 10.0).

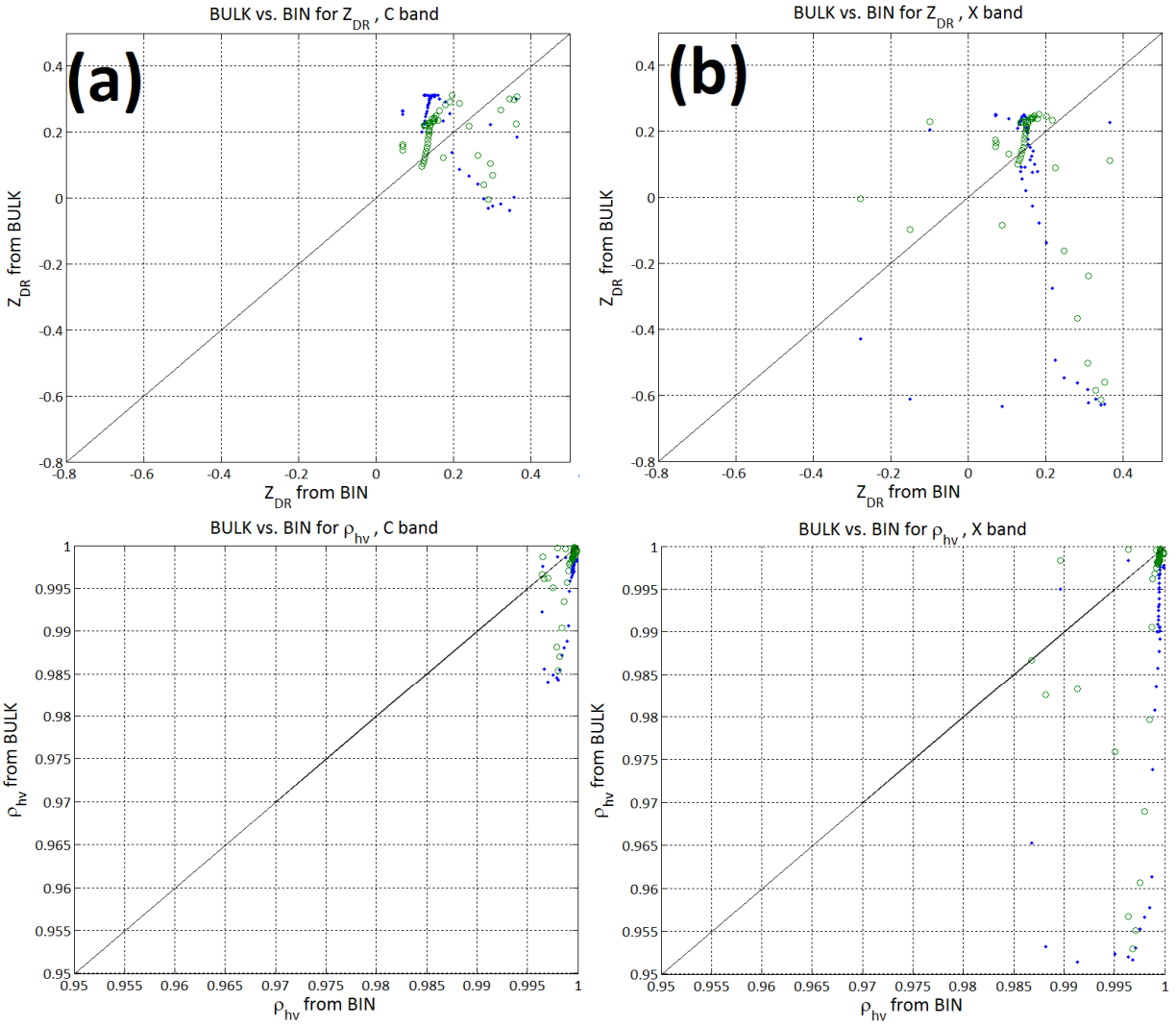

Fig. 12: Bulk versus bin model Z_{DR} and ρ_{hv} for (a) C band (left column) and (b) X band (right column). Blue points are for one-moment hail size distributions (HSDs), green circles are for two-moment HSDs. Fixed shape parameter $\alpha = 0$. Distributions come from an altitude of 4.65 km AGL and hailstones are dry.

upon backscatter[2] (δ). Particle size distributions encompassing the band of sizes near these Mie scatterers contribute large variations in δ to the backscattered signal, reducing ρ_{hv}. An example of how the bulk schemes with fixed $\alpha = 0$ overcount the Mie scatterers is given in Fig. 13. Note that the smaller resonance size at X band (and thus larger concentration of these particles) accounts for the larger reduction in ρ_{hv} and more negative Z_{DR} values in Fig. 12. Overcounting large particles can be mitigated by constraining the bulk PSDs with larger shape parameters, effectively narrowing the spectrum. The tradeoff of a narrower spectrum would likely be the undercounting of smaller hailstones, leading to underestimations of Z_H. At S band the resonance size is quite large (6.16 cm), so negative Z_{DR} and reduced ρ_{hv} values owing to overcounting are not a significant problem. In fact, bulk model Z_H at S band better matches those of the bin model for smaller shape parameters (not shown).

The error characteristics of the hail size distributions are quite different closer to the surface. Melting of hailstones can act to truncate the particle size distribution as the smaller stones melt rapidly into raindrops. Fixed intercept parameters in 1M bulk schemes cannot capture this effect, and 2M schemes with a fixed shape parameter α may also have difficulty capturing a narrowing distribution. Small

[2] Nonzero values of backscatter differential phase arise from Mie scatterers that have some degree of alignment. In other words, if the particles are chaotically oriented, scattering is isotropic and thus backscatter differential phase is zero.

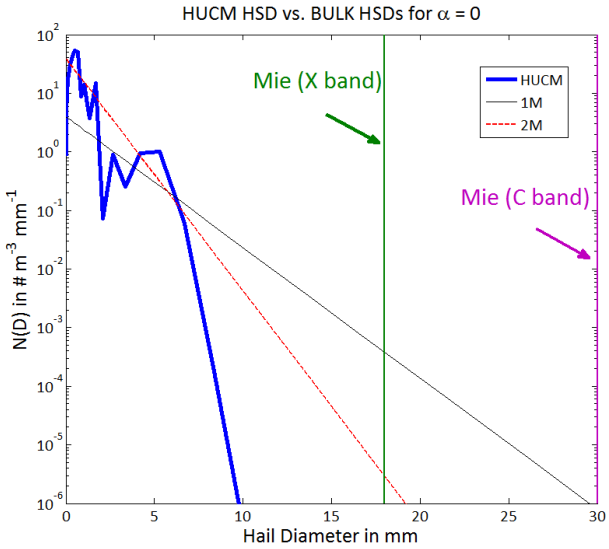

Fig. 13: An example hail size distribution from the HUCM (blue, thick curve) and the corresponding 1M (black) and 2M (red) DSDs, constrained by a fixed α = 0. The green (magenta) vertical bars indicate the resonance size for X band (C band).

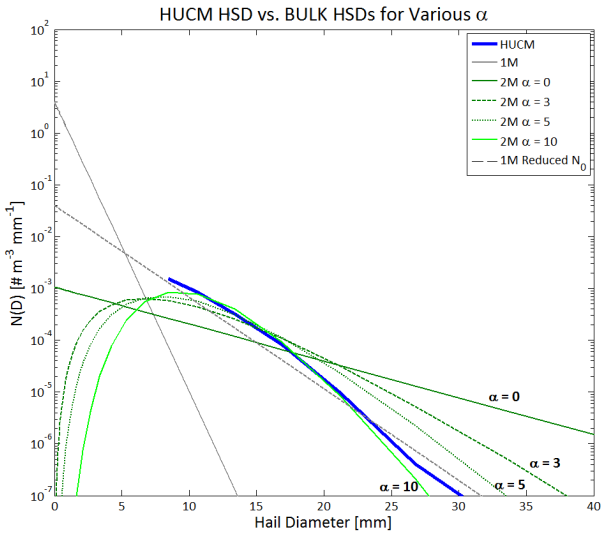

Fig. 14: Low-level hail size distributions from the HUCM (thick blue line) and various bulk scheme assumptions, including 1M (solid gray curve); 1M with reduced intercept parameter, dashed gray curve), and 2M schemes with various shape paremeters (α = 0, dark green solid line; α = 3, dashed dark green line; α = 5, dotted dark green line; α = 10, solid light green line).

values of α result in excessive concentrations of both the smallest and largest particle sizes (e.g., Fig. 14), which provide erroneously large estimates of Z_H.

Before performing scattering calculations for the melting hailstones, it is worth mentioning that some bulk microphysics schemes (e.g., MY05b, MY06a) consider melting hailstones to be *dry* when calculating Z_H. The justification given for this physical inconsistency is that the Z_H values are in better agreement with observations when hailstones are assumed dry. The reason for the apparent discrepancy between observations (in which hailstones are undoubtedly wet) and the model calculations is the oversimplified method used to calculate the radar variables. In the MY scheme, all particles are considered to be Rayleigh scatterers when calculating the equivalent radar reflectivity factor[3]. This assumption is worst at shorter radar wavelengths, at which most melting hailstones are out of the Rayleigh scattering regime. In reality, such non-Rayleigh scattering can result in lower Z_H values than are obtained using the Rayleigh approximation, which is why MY use dry Rayleigh scatterers in their calculations. However, a more appropriate method involves more rigorous treatment of particle scattering using T-matrix calculations (e.g., Jung et al. 2010; Ryzhkov et al. 2011).

In the HUCM, hailstones are considered solid ice (density ρ_i = 917 kg m^{-3}), so the melted water collects on the exterior of the particle in a "coat" until sufficient mass has accumulated that shedding of excess meltwater commences, following the model of melting hail by Rasmussen and Heymsfield (1987). The HUCM provides the maximum liquid water mass fraction on melting hailstones at each grid cell, which is used to determine the thickness of the water coat on each hailstone size. Note that the maximum amount of meltwater mass allowable before the onset of shedding is dependent on the size of the hailstone and is thus different for each size bin. This is in contrast to schemes such as F94, where the maximum liquid water fraction is uniform across the size spectrum. Schemes such as Meyers et al. (1997), which use the Rasmussen and Heymsfield shedding condition, are more physical in this regard. Owing to the melting-induced truncation of the distribution, Z_H is overpredicted for the 2M distribution with α = 0, whereas α = 10.0 provides a much better fit to the bin distribution Z_H values (Fig. 15). The 1M scheme mainly underpredicts Z_H, except for very heavy hailfall. Whereas the magnitude of the relative errors in Z_H decreases with increasing shape parameter, the relative errors in Z_{DR} do not change monotonically with α (Fig. 16). In fact, errors in Z_{DR} are larger for α

[3] There is a typographical error in MY05b's definition of the equivalent radar reflectivity factor Z_e: the expression given is for Rayleigh ice particles, not for all particles of any composition, as they state. See Smith et al. (1984).

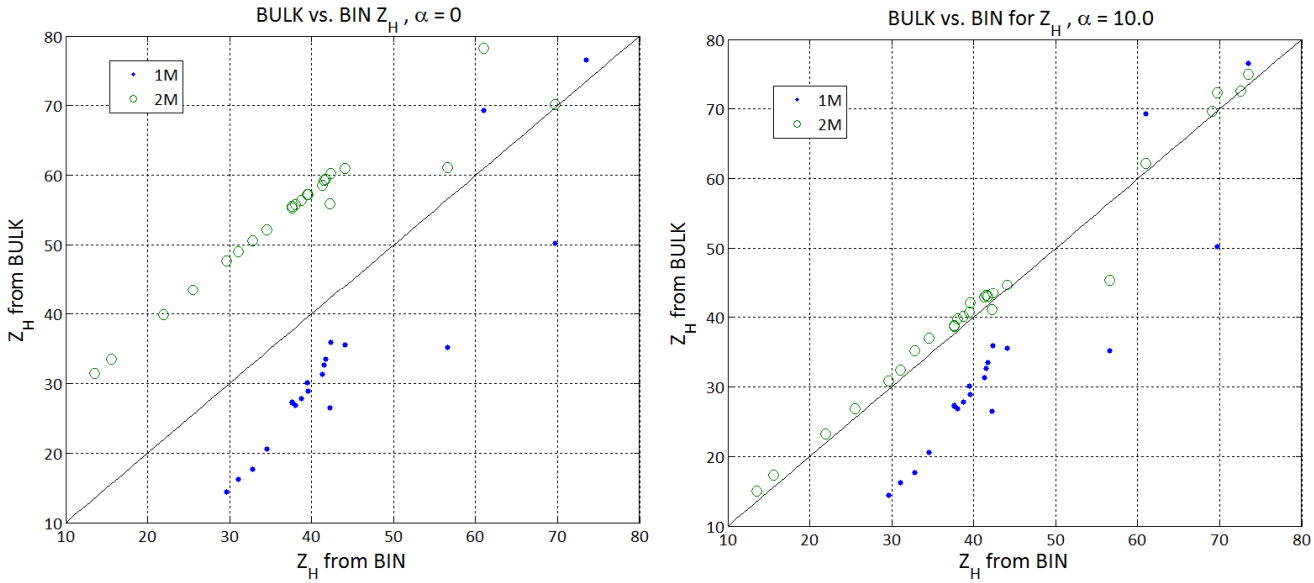

Fig. 15: Comparison of S-band Z_H for melting hailstones computed from the bin hail size distribution versus the Z_H computed from the bulk distributions (blue points are for 1M scheme assumptions, green circles for 2M scheme assumptions). Shape parameters were fixed at α = 0 (left panel) and α = 10.0 (right panel).

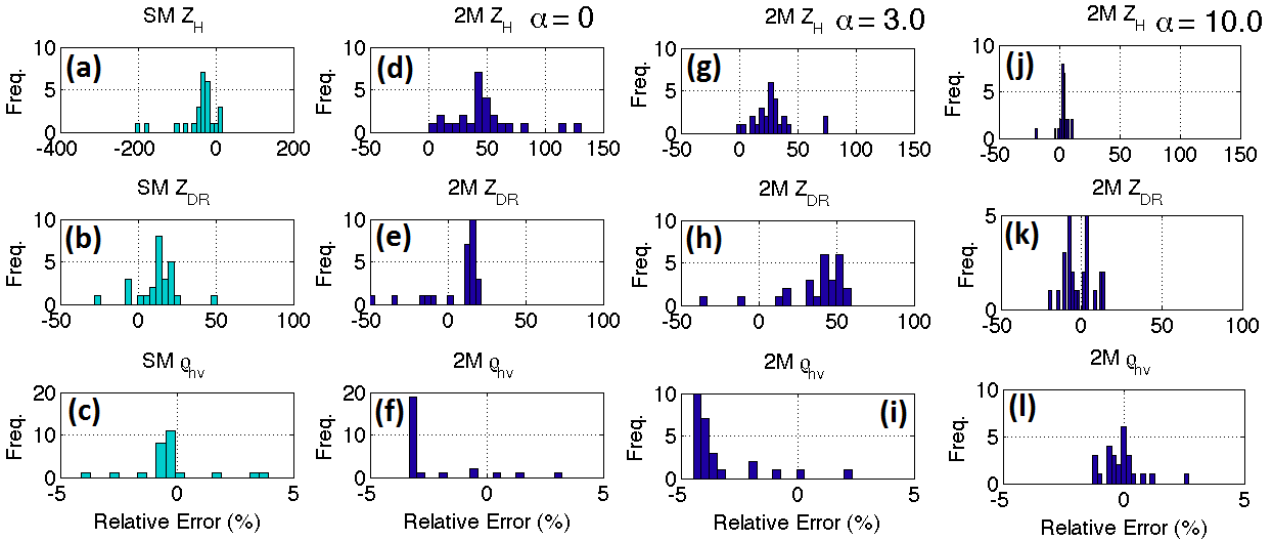

Fig. 16: Histograms of relative errors in the melting hail polarimetric radar variables (compared to the HUCM) computed from various bulk microphysics scheme distributions: (a) – (c):1M PSDs; (d) - (f) 2M distributions with fixed α = 0; (g) – (i) 2M distributions with fixed α = 3.0; (j) – (l) 2M distributions with fixed α = 10.0. Variables calculated are (from top to bottom) Z_H, Z_{DR}, and ρ_{hv}. The abscissa axis on each 2M plot is the same for ease of comparison.

= 3.0 (> 50%) than for $\alpha = 0$ or $\alpha = 10.0$, with $\alpha = 10.0$ providing the smallest relative errors (no more than ± 20%). The errors in ρ_{hv} are also minimized for $\alpha = 10.0$ (generally no more than ±2%). Such non-monotonicity reveals how sensitive the polarimetric variables are to changes in the shape of the PSD, especially changes affecting the relative concentrations of the larger particles. Also note the general decrease in the width of the relative error frequency distributions with increasing α; constraining the PSD with a large shape parameter effectively limits the amount of variability in the distribution, constraining the range of realizable polarimetric variables.

8. DISCUSSION AND CONCLUSIONS

The results demonstrating the deficiencies of bulk microphysics parameterization schemes in simulating the polarimetric radar variables in situations of ongoing size sorting or other processes that preferentially affect only part of the PSD have implications for attempts to assimilate polarimetric radar data. For example, because of the inability of 1M schemes to produce size sorting, assimilation of Z_{DR} into a storm-scale model using such a scheme will likely increase analysis errors in cases of size sorting (e.g., Jung et al. 2010). This is because, in the framework of a SM scheme, there is a one-to-one correspondence between the assimilated observation (Z_{DR}) and the predicted model variable (e.g., rain mass mixing ratio q_r). Thus, regions of high Z_{DR} correspond to larger q_r. In the case of size sorting, the model would adjust to the high-Z_{DR} observation by incorrectly increasing rain mass at that location, which is exactly opposite of the physical situation. The incorrect inclusion of additional water mass can affect other processes such as evaporation, which has ramifications for the development and strength of cold pools (e.g., Dawson et al. 2010). Therefore, if using SM microphysics schemes in assimilation experiments where size sorting may be prevalent (e.g., supercells or other deep moist convection), it is best *not* to use Z_{DR} data.

As discussed above, double-moment schemes with fixed shape parameter (α) can suffer from excessive size sorting. For this reason, diagnostic-α techniques (e.g., MY05a,b; Milbrandt and McTaggart-Cowan 2010; Mansell 2010) were developed. In MY05a,b and Milbrandt and McTaggart-Cowan (2010), α increases with increasing mean-mass diameter D_m to reflect the narrowing of DSDs undergoing size sorting. Z_{DR} offers an attractive observation that can be related to D_m; of course, high Z_{DR} (and large D_m) alone does not necessarily mean size sorting is occurring. Therefore, it may be desirable to "flag" areas of the storm where size sorting may be occurring using Z_H and Z_{DR} observations, thereby limiting the use of such diagnostic-α relations only to regions where they are necessary. Such a flagging system could make use of predetermined Z_H and Z_{DR} thresholds, or locations in which the Z_H and Z_{DR} data exhibit a strong negative correlation.

How one treats the large-particle tail of the PSD is extremely important for polarimetric radar applications. Single-moment and double-moment schemes with fixed shape parameter create large errors in the computed polarimetric variables for a number of microphysical processes, including size sorting, evaporation, freezing, and melting. Instead, allowing α to vary is essential for reducing errors in mapping model output to dual-polarization radar variables (or vice versa in the case of data assimilation). Based on our error analysis using the 3M scheme for size sorting, it is recommended that such 3M schemes (or diagnostic-α 2M schemes) be used with a constraint on the maximum allowable α (α_{max} no more than 20 – 30). While not perfect, such schemes that allow for variable shape parameters minimize the errors in cases where microphysical processes narrow the PSD (e.g., size sorting, evaporation, melting of hailstones, etc.). In this way, more effective blending of storm-scale numerical weather prediction models and polarimetric radar data can be achieved, ultimately improving model analyses and short-term forecasts.

9. ACKNOWLEDGMENTS

The first author would like to thank the members of his doctoral committee for feedback on portions of this work, which stemmed from the Doctoral General Exam at OU. This work has benefited from useful discussions with Dan Dawson (NSSL) and Alex Schenkman (OU). Partial funding from this work comes from the NOAA/Office of Oceanic and Atmospheric Research under NOAA-University of Oklahoma Cooperative Agreement NA17RJ1227, U.S. Department of Commerce.

10. REFERENCES

Bigg, E.K., 1953: The formation of atmospheric ice crystals by the freezing of droplets. *Q. J. Roy. Meteor. Soc.*, **79**, 510-519.

Brandes, E.A., G. Zhang, and J. Vivekanandan, 2002: Experiments in rainfall estimation with a polarimetric radar in a subtropical environment. *J. Appl. Meteor.*, **41**, 674-685.

Bringi, V.N., K. Knupp, A. Detwiler, L. Liu, I.J. Caylor, and R.A. Black, 1997: Evolution of Florida thunderstorms during the Convection and Precipitation Electrification Experiment: The case of 9 August 1991. *Mon. Wea. Rev.*, **125**, 2131-2160.

Cao, Q., G. Zhang, E. Brandes, T. Schuur, A. V. Ryzhkov, and K. Ikeda, 2008: Analysis of video disdrometer and polarimetric radar data to characterize rain microphysics in Oklahoma. *J. Appl. Meteor. and Climatol.*, **47**, 2238–2255.

Clabo, D.R., A.G. Detwiler, and P.L. Smith, 2009: Polarimetric radar signatures of hydrometeors observed within mature convective storms. *Extended Abstracts*, 34th Conf. on Radar Meteorology, Amer. Meteor. Soc., Williamsburg, VA, P13.5.

Cotton, W.R., M.A. Stephens, T. Nehrkorn, and G.J. Tripoli, 1982: The Colorado State University three-dimensional cloud/mesoscale model-1982: Part II: An ice phase parameterization. *J. Rech. Atmos.*, **16**, 295-320.

Cotton, W.R., G.J. Tripoli, R.M. Rauber, and E.A. Mulvihill, 1986: Numerical simulation of the effects of varying ice crystal nucleation rates and aggregation processes on orographic snowfall. *J. Clim. Appl. Meteor.*, **25**, 1658-1680.

Dawson, D.T., M. Xue, J.A. Milbrandt, and M.K. Yau, 2010: Comparison of evaporation and cold pool development between single-moment and multi-moment bulk microphysics schemes in idealized simulations of tornadic thunderstorms. *Mon. Wea. Rev.*, **138**, 1152-1171.

Doviak, R.J. and D.S. Zrnić, 1993: *Doppler Radar and Weather Observations*. Academic Press, 562 pp.

Federer, B. and A. Waldvogel, 1975: Hail and raindrop size distributions from a Swiss multicell storm. *J. Appl. Meteor.*, **14**, 91-97.

Ferrier, B.S., 1994: A double-moment multiple-phase four-class bulk ice scheme. Part I: Description. *J. Atmos. Sci.*, **51**, 249-280.

Ferrier, B.S., W.-K. Tao, and J. Simpson, 1995: A double-moment multiple-phase four-class bulk ice scheme. Part II: Simulations of convective storms in different large-scale environments and comparisons with other bulk parameterizations. *J. Atmos. Sci.*, **52**, 1001-1033.

Gunn, K.L.S., and J.S. Marshall, 1958: The distribution with size of aggregate snowflakes. *J. Meteor.*, **15**, 452-461.

Hubbert, J.C., V.N. Bringi, L.D. Carey, and S. Bolen, 1998: CSU-CHILL polarimetric radar measurements from a severe hail storm in eastern Colorado. *J. Appl. Meteor.*, **37**, 749-775.

Jameson, A.R., M.J. Murphy, and E.P. Krider, 1996: Multiple parameter radar observations of isolated Florida thunderstorms during the onset of electrification. *J. Appl. Meteor.*, **35**, 343-354.

Jung, Y., G. Zhang, and M. Xue, 2008a: Assimilation of simulated polarimetric radar data for a convective storm using the Ensemble Kalman Filter. Part I: Observation operators for reflectivity and polarimetric varaibles. *Mon. Wea. Rev.*, **136**, 2228-2245.

Jung, Y., M. Xue, and G. Zhang, 2010: Simulations of polarimetric radar signatures of a supercell storm using a two-moment bulk microphysics scheme. *J. Appl. Meteor. and Climatol.*, **49**, 146-163.

Kessler, E., 1969: *On the Distribution and Continuity of Water Substance in Atmospheric Circulations*. Meteor. Monogr. No. 32, Amer. Meteor. Soc., 84 pp.

Khain, A., A. Pokrovsky, M. Pinsky, A. Seifert, and V. Phillips, 2000: Notes on the state-of-the art numerical modeling of cloud microphysics. *Atmos. Res.*, **55**, 159-224.

Khain A., A. Pokrovsky and M. Pinsky, A. Seifert, and V. Phillips, 2004: Effects of atmospheric aerosols on deep convective clouds as seen from simulations using a spectral microphysics mixed-phase cumulus cloud model Part 1: Model description. *J. Atmos. Sci.,* **61***,* 2963-2982.

Kumjian, M.R., and A.V. Ryzhkov, 2009: Storm-relative helicity revealed from polarimetric radar measurements. *J. Atmos. Sci.*, **66**, 667-685.

Kumjian, M.R., and A.V. Ryzhkov 2010: The impact of evaporation on polarimetric characteristics of rain: Theoretical model and practical implications. *J. Appl. Meteor. and Climatol.,* **49**, 1247-1267.

Kumjian, M.R., and A.V. Ryzhkov, 2012: The impact of size sorting on the polarimetric radar variables. *J. Atmos. Sci.*, **conditionally accepted.**

Kumjian, M.R., S. Ganson, and A.V. Ryzhkov, 2010a: Polarimetric characteristics of freezing drops:

Theoretical model and observations. *5th European Conf. on Radar in Meteorology and Hydrology*, Sibiu, Romania.

Kumjian, M.R., J.C. Picca, S.M. Ganson, A.V. Ryzhkov, J. Krause, and A.P. Khain, 2010b: Polarimetric radar characteristics of large hail. *25th Conf. on Severe Local Storms*, Denver, CO, Amer. Meteor. Soc., 11.2.

Lin, Y.-L., R.D. Farley, and H.D. Orville, 1983: Bulk parameterization of the snow field in a cloud model. *J. Clim. Appl. Meteor.*, **22**, 1065-1089.

Loney, M.L., D.S. Zrnic, J.M. Straka, and A.V. Ryzhkov, 2002: Enhanced polarimetric radar signatures above the melting level in a supercell storm. *J. Appl. Meteor.*, **41**, 1179-1194.

Marshall, J.S., and W. Mc K. Palmer, 1948: The distribution of raindrops with size. *J. of Meteor.*, **5**, 165-166.

Meyers, M.P., R.L. Walko, J.Y. Harrington, and W.R. Cotton, 1997: New RAMS cloud microphysics parameterization. Part II: The two-moment scheme. *Atmos. Res.*, **45**, 3-39.

Milbrandt, J.A., and M.K. Yau, 2005a: A multimoment bulk microphysics parameterization. Part I: Analysis of the role of the spectral shape parameter. *J. Atmos. Sci.*, **62**, 3051-3064.

Milbrandt, J.A., and M.K. Yau, 2005b: A multimoment bulk microphysics parameterization. Part II: A proposed three-moment closure scheme and description. *J. Atmos. Sci.*, **62**, 3065-3081.

Milbrandt, J.A., and M.K. Yau, 2006a: A multimoment bulk microphysics parameterization. Part III: Control simulation of a hailstorm. *J. Atmos. Sci.*, **63**, 3114-3136.

Milbrandt, J.A., and M.K. Yau, 2006b: A multimoment bulk microphysics parameterization. Part IV: Sensitivity experiments. *J. Atmos. Sci.*, **63**, 3137-3159.

Milbrandt, J.A., and R. McTaggart-Cowan, 2010: Sedimentation-induced errors in bulk microphysics schemes. *J. Atmos. Sci.*, **67**, 3931-3948.

Murakami, M., 1990: Numerical modeling of dynamical and microphysical evolution of an isolated convective cloud – the 19 July 1981 CCOPE cloud. *J. Meteor. Soc. of Japan*, **68**, 107-128.

Ogura, Y., and T. Takahashi, 1973: The development of warm rain in a cumulus model. *J. Atmos. Sci.*, **30**, 262-277.

Pfeifer, M., G.C. Graig, M. Hagen, and C. Keil, 2008: A polarimetric radar forward operator for model evaluation. *J. Appl. Meteor. and Climatol.*,**47**, 3202-3220.

Picca, J.C., M.R. Kumjian, and A.V. Ryzhkov, 2010: Z_{DR} columns as a predictive tool for hail growth and storm evolution. Extended Abstracts, *25th Conference on Severe Local Storms*, American Meteorological Society, Denver, Colorado, 11.3.

Pruppacher, H.R., Klett, J.D., 1997: *Microphysics of Clouds and Precipitation*. 2nd ed. Kluwer Academic, 348 pp.

Rasmussen, R. M., and A. J. Heymsfield, 1987: Melting and shedding of graupel and hail. Part I: Model physics. *J. Atmos. Sci.*, **44,** 2754–2763.

Reisner, J., R.M. Rasmussen, and R.T. Bruintjes, 1998: Explicit forecasting of supercooled liquid water in winter storms using the MM5 mesoscale model. *Q. J. Roy. Meteor. Soc.*, **124**, 1071-1107.

Rogers, R. R., and M. K. Yau, 1989: *A Short Course in Cloud Physics*. 3rd ed. Elsevier Press, 290 pp.

Ryzhkov, A.V., M. Pinsky, A. Pokrovsky, and A. Khain, 2011: Polarimetric radar observation operator for a cloud model with spectral microphysics. *J. Appl. Meteor. and Climatol.*, **50**, 873-894.

Smith, P.L., 1984: Equivalent radar reflectivity factors for snow and ice particles. *J. Clim. Appl. Meteor.*, **23**, 1258-1260.

Smith, P.L., D.J. Musil, A.G. Detwiler, and R. Ramachandran, 1999: Observations of mixed-phase precipitation within a CaPE Thunderstorm. *J. Appl. Meteor.*, **38**, 145-155.

Straka, J.M., and E.R. Mansell, 2005: A bulk microphysics parameterization with multiple ice precipitation categories. *J. Appl. Meteor.*, **44**, 445-466.

Thériault, J.M. and R.E. Stewart, 2010: A parameterization of the microphysical processes forming many types of winter precipitation. *J. Atmos. Sci.*, **67**, 1492-1508.

Thompson, G., R.M. Rasmussen, and K. Manning, 2004: Explicit forecasts of winter precipitation using an improved bulk microphysics scheme. Part I: Description and sensitivity analysis. *Mon. Wea. Rev.*, **132**, 519-542.

Ulbrich, C.W., 1983: Natural variations in the analytical form of the raindrop size distribution. *J. Clim. Appl. Meteor.*, **22**, 1764-1775.

Uplinger, W.G., 1981: A new formula for raindrop terminal velocity. *Proc. 20th Conf. on Radar Meteorology*, Boston, Amer. Meteor. Soc., 389-391.

Wacker, U. and A. Seifert, 2001: Evolution of rain water profiles resulting from pure sedimentation: Spectral vs. parameterized description. *Atmos. Res.*, **58**, 19-39.

Walko, R., W.R. Cotton, M.P. Meyers, and J.Y. Harrington, 1995: New RAMS cloud microphysics parameterization. Part I: The single-moment scheme. *Atmos. Res.*, **38**, 29-62.

Wisner, C., H.D. Orville, and C. Meyers, 1972: A numerical model of a hail-bearing cloud. *J. Atmos. Sci.*, **29**, 1160-1181.

Zhang, G., J. Vivekanandan, and E.A. Brandes, 2001: A method for estimating rain rate and drop size distribution from polarimetric radar measurements. *IEEE Trans. Geosci. Rem. Sens.*, **39**, 830-841.

Ziegler, C.L., 1985: Retrieval of thermal and microphysical variables in observed convective storms. Part I: Model development and preliminary testing. *J. Atmos. Sci.*, **42**, 1487-1509.